CHEMISTRY OF MATERIALS

Article

pubs.acs.org/cm

DFT Study of the Role of Al^{3+} in the Fast Ion-Conductor $Li_{7-3x}Al^{3+}{}_xLa_3Zr_2O_{12}$ Garnet

Daniel Rettenwander,*[,†] Peter Blaha,[‡] Robert Laskowski,[§] Karlheinz Schwarz,[‡] Patrick Bottke,[∥] Martin Wilkening,[∥] Charles A. Geiger,[†] and Georg Amthauer[†]

[†]Department of Materials Research and Physics, University of Salzburg, 5020 Salzburg, Austria

[‡]Institute of Materials Chemistry, Vienna University of Technology, 1060 Vienna, Austria

[§]Institute of High Performance Computing, Agency for Science, Technology, and Research (A*STAR), 138632 Singapore

[∥]Christian Doppler Laboratory for Lithium Batteries, Institute for Chemistry and Technology of Materials, Graz University of Technology, 8010 Graz, Austria

ABSTRACT: We investigate theoretically the site occupancy of Al^{3+} in the fast-ion-conducting cubic-garnet $Li_{7-3x}Al^{3+}{}_xLa_3Zr_2O_{12}$ (*Ia*-3*d*) using density functional theory. By comparing calculated and measured ^{27}Al NMR chemical shifts an analysis shows that Al^{3+} prefers the tetrahedrally coordinated 24*d* site and a distorted 4-fold coordinated 96*h* site. The site energies for Al^{3+} ions, which are slightly displaced from the exact crystallographic sites (i.e., 24*d* and 96*h*), are similar leading to a distribution of slightly different local oxygen coordination environments. Thus, broad ^{27}Al NMR resonances result reflecting the distribution of different isotropic chemical shifts and quadrupole coupling constants. From an energetic point of view, there is evidence that Al^{3+} could also occupy the 48*g* site with its almost regular octahedral coordination sphere. Although this has been reported by neutron powder diffraction, the NMR chemical shift calculated for such an Al^{3+} site has not been observed experimentally.

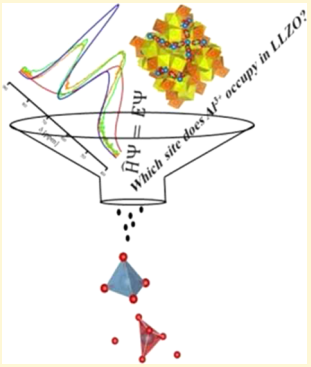

INTRODUCTION

The fast Li-ion conductor with the nominal composition $Li_7La_3Zr_2O_{12}$ (LLZO) is receiving much scientific attention since its discovery in 2007.[1] It has a garnet-based structure, and it occurs in at least two structural modifications.[2,3] At room temperature, LLZO is tetragonal ($I4_1/acd$) while the cubic modification (*Ia*-3*d*) is stable above approximately 150 °C.[4] Geiger et al. argued that the better conducting cubic phase can be stabilized at room temperature (RT) through the incorporation of small amounts of Al^{3+}.[4] The stabilizing effect of Al^{3+} has now been confirmed by a number of subsequent investigations.[5−19] The exact role Al^{3+} plays in cubic Al-bearing LLZO is important because LLZO shows a high ionic conductivity of about 10^{-4} S/cm at RT. This is approximately 2 orders of magnitude higher than that for the lower symmetry Al-free tetragonal LLZO phase. LLZO also has good chemical and thermal stability, as well as a wide energy potential window making it an excellent candidate for use as an electrolyte in an all-solid-state lithium-ion battery.[1,20]

As has been shown recently, ionic conductivity also seems to depend on the amount of Al^{3+} incorporated during synthesis.[6,8] Further work, however, is needed to quantify this effect. For this purpose, the chemical and physical properties governing Li^+ diffusion have to be understood in detail; in particular this includes the important question as to which crystallographic sites the Al^{3+} ions preferably occupy in the cubic phase of LLZO.

Considerable experimental research has been undertaken to obtain information about Al^{3+} in LLZO, including its local coordination and site partitioning behavior. In this context, ^{27}Al magic angle spinning (MAS) nuclear magnetic resonance (NMR) spectroscopy is a key method. Several NMR studies have proposed that the resonance observed at a chemical shift ranging from 64 to 68 ppm corresponds to Al^{3+} located at the "standard garnet" tetrahedral site.[4−7] There is uncertainty, however, about the interpretation and assignment of the other measured NMR lines that have chemical shifts ranging from approximately 78 to 82 ppm. The interpretations given so far include Al^{3+} residing at nontetrahedral Li^+ sites (4-fold to possibly 6-fold coordinated) and tetrahedrally coordinated sites in the neighborhood of La^{3+} or Zr^{4+} vacancies in Al-rich LLZO.[4,5] In particular, mechanochemically prepared LLZO samples with a high amount of Al^{3+}, but reduced in La^{3+} and Zr^{4+} content, even indicate two magnetically inequivalent tetrahedral sites.[6] Neutron powder diffraction (NPD) measurements were interpreted as indicating that Al^{3+} is located at an octahedrally coordinated site in the garnet framework.[11]

Summarizing the various published experimental results, there is no clear understanding as to which sites are occupied by Al^{3+} in cubic LLZO. This also concerns the detailed interpretation of ^{27}Al NMR MAS spectra and diffraction results.

Received: January 10, 2014
Revised: March 13, 2014
Published: March 19, 2014

To address the important role of Al^{3+} in LLZO and to obtain a better understanding of the various experimental results, we undertook a density functional theory (DFT) investigation of Al-bearing cubic LLZO with the aim to calculate (relative) ^{27}Al NMR parameters such as chemical shifts and electric quadrupole coupling constants.

COMPUTATIONAL METHODS

In order to understand the computational models used in this investigation, we provide a short description of the crystal structure of cubic LLZO garnet (Figure 1).

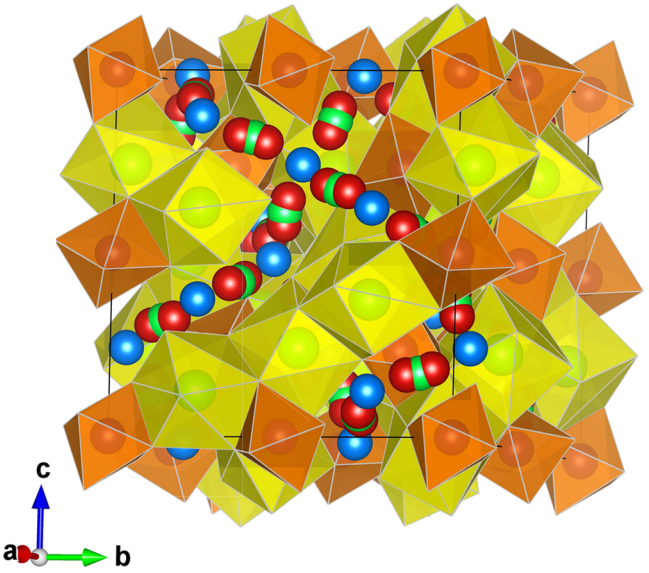

Figure 1. Crystal structure of cubic LLZO. The yellow dodecahedrally coordinate La^{3+} (at the Wyckoff position 24*c*) and orange octahedrally coordinate Zr^{4+} (16*a*). The blue spheres correspond to tetrahedrally coordinated (24*d*) Li^+, green spheres to octahedrally coordinated (48*g*) Li^+, and red ones to distorted 4-fold coordinated (96*h*) Li^+.

"Garnet" is the common name for a large number of natural and synthetic metal oxide and fluoride phases.[21] Conventional oxide garnets have the general formula $A_3B_2C_3O_{12}$ and crystallize with cubic symmetry *Ia*-3*d*. In the case of LLZO, the O^{2-} ions, located at general crystallographic positions, 96*h*, form an oxygen-ion framework with interstices occupied by the A cations (La^{3+}) at an 8-fold coordinated position 24*c* (point symmetry 222), by B cations (Zr^{4+}) at a 6-fold coordinated position 16*a* (point symmetry −3), and by C cations (Li^+) at a 4-fold coordinated 24*d* position (point symmetry −4). In addition to these cation sites, there are other interstices within the oxygen framework that are empty in the conventional garnet structure,[22] such as the 6-fold coordinated 48*g* positions (point symmetry 2) and a general 96*h* position, sometimes described as 4-fold coordinated with two additional longer bonds greater than 2.8 Å in length,[23] 5-fold[4] coordinated or 6-fold[11] coordinated (point symmetry 1). These interstices can be filled by "extra" cations (such as Li^+), giving rise to compositions with nonstandard garnet stoichiometry. An important property is the partial occupancy of the structural sites (24*d*, 48*g*, and 96*h*) where Li^+ is located and also delocalization of Li^+ ions throughout.

Several theoretical DFT studies on LLZO have been published before.[24−29] They concentrate on the basic structural properties and on the Li^+ diffusion, but none of them considers Al^{3+} ions explicitly.

For our first-principle calculations, the ions in LLZO were arranged on the basis of crystal structure descriptions in the literature.[24] Three different structural models were used with all having a body centered (*I*-type) Bravais lattice with $a = b = c = 12.972$ Å and $\alpha = \beta = \gamma = 90°$. Three garnet compositions were chosen, namely $Li_{44}Al_4La_{24}Zr_{16}O_{96}$ with Al^{3+} at 24*d*, 48*g* and 96*h*, $Li_{56}Al_4La_{20}Zr_{16}O_{96}$ with Al^{3+} solely at 24*c*, and $Li_{60}Al_4La_{24}Zr_{12}O_{96}$ with Al^{3+} solely at 16*a*. The Li^+ ions were distributed over the 24*d* and the 96*h* sites following Xu et al.[25] No significant effect on the results was observed by choosing a different Li^+ arrangement. The highest symmetry possible was maintained to save computational costs. The first model was used to understand the behavior of Al^{3+} at various possible sites occupied by Li^+. The calculations were made with 17 different local Al^{3+} positions located among the 24*d*, 96*h*, and 48*g* sites. To avoid cation repulsion, all Li^+ ions close to Al^{3+} were removed. The various Al^{3+} positions were fixed during relaxation and all Al^{3+} ions are equivalent in the unit cell.

All calculations are based on DFT methods using the all-electron full potential linearized augmented plane wave (LAPW) method as implemented in the Wien2k code.[30,31] The Perdew Burke Ernzerhof (PBE) generalized gradient approximation (GGA) was employed.[32] The atomic positions were optimized by minimization of the forces (below 2 mRy/au) acting on the atoms simultaneously with the self-consistent-field cycle as implemented by Marks.[33] The eigenvalue problem was solved by an "iterative diagonalization" using an efficient preconditioning (inverse of H - λS) and the block-Davidson method.[34] The radii of the atomic spheres (R_{MT}) for the Li^+, La^{3+}, Zr^{4+}, O^{2-}, and Al^{3+} ions were chosen to be 1.46, 2.27, 1.93, 1.71, and 1.40 au, respectively. The cutoff for the plane wave $R_{MT}K_{max} = 6.0$ and the maximum Fourier expansion of charge density cutoff $G_{max} = 12$ (au)$^{-1}$ were applied. The separation parameter between the valence and core states was chosen to be −6.0 Ry. We used 1 *k*-points in the irreducible Brillouin zone. The computational considerations were checked by increasing $R_{MT}K_{max}$ and the number of *k*-points, but no significant changes with respect to the energy, geometry, and the electric field gradient (EFG) around Al^{3+} were observed.

The behavior of Al^{3+} at different crystallographic sites was analyzed qualitatively by weighing the various Al^{3+} positions, x_i, with their corresponding energy, $E(x_i)$. The various local energies for Al^{3+} at and around the crystallographic positions where Li can also be located, were described by fitting a polynomial, describing a possible diffusion pathway. The ocuppation probabilities for an Al^{3+} ion along this path are described using a normalized Boltzmann factor given by

$$W(x_i) = \begin{cases} i = 0 \rightarrow & \dfrac{1 - e^{-\Delta E(x_{i+1},x_i)/kT}}{\sum_i^n W(x_i)} =: \text{minimum} \\ i = 1 \rightarrow & \dfrac{e^{-\Delta E(x_{i+1},x_i)/kT} - e^{\Delta E(x_{i-1},x_{i+1})/kT}}{\sum_i^n W(x_i)} \\ i > 1 \rightarrow & \dfrac{W(x_{i-1})\, e^{-\Delta E(x_i,x_{i-1})/kT} - W(x_{i-1})\, e^{\Delta E(x_{i-1},x_{i+1})}}{\sum_i^n W(x_i)} \end{cases}$$

$$\forall\, x_i \in x_i | E(x_i) \Lambda E(x_{i-1}) < E(x_i) < E(x_{i+1})$$

where k is Boltzmann's constant, and where x_{i+1} indicates the states next to x_i, x_{i-1} indicates the states before x_i with an interval of 0.01 Å, and T is 298.15 K. The site preference energy, ΔE, is defined as $\Delta E = E(x_i) - E^{global}$, where E^{global} is the global energy minimum and corresponds to Al^{3+} located at 24*d*. It has the lowest total energy for all the calculated arrangements of Al in LLZO.

In NMR spectroscopy, the chemical shift, δ, of a nucleus, i, describes the nuclear shielding effect of an applied (external) static magnetic field and the locally induced magnetic field arising from the surrounding electrons with a certain probability of presence near the corresponding nuclear site i. The magnitude of the resulting effective field, B_{eff}, is given by $B_{eff} = B_0(\mathbf{1} - \sigma_i)$, where σ_i is a second-rank nuclear shielding tensor, $\mathbf{1}$ is the unit matrix and B_0 is a uniform external field along the z-axis. The resonance NMR frequency, ν_i, is then given by $\nu_i = (\gamma_i/2\pi)\, B_{eff}$, where γ_i is the magnetogyric ratio of the nucleus under observation. The isotropic chemical shift, δ_{iso} (henceforth δ), describes the relation between the NMR resonance frequency for the nucleus of interest, ν_i, and the corresponding resonance frequency for a reference compound, ν_{ref}, giving $\delta = 10^6 \times (\nu_i - \nu_{ref})/\nu_{ref}$. Because of the orientation in systems with periodic boundary conditions, all anisotropic interactions causing line broadening are

dx.doi.org/10.1021/cm5000999 | *Chem. Mater.* 2014, 26, 2617−2623

projected onto the axis of rotation where they collapse at the magic angle.[35] To compute δ, we used the relaxed geometry and applied the NMR module[36−38] of the Wien2k code.[31] These chemical shift calculations are based on an all-electron linear response method where one obtains the induced current density considering the perturbation of the ground state wave functions due to the external magnetic field. The resulting magnetic shielding is then obtained by integration of the all-electron current according to Biot−Savart's law without further approximations. Because there is agreement in the literature[4−7] that the ^{27}Al NMR resonance at 66 ± 2 ppm represents tetrahedrally coordinated Al^{3+} at 24*d* in LLZO (δ_{24d} = 68 ppm), we calculate the difference of the chemical shifts ($\Delta\delta$) for Al^{3+} at other positions x_i with a δ_{xi} as follows

$$\Delta\delta = \delta_{x_i} - \delta_{24d}$$

Besides the chemical shift, the interaction of the quadrupole moment, *Q*, of the ^{27}Al nucleus (spin-quantum number $I = 5/2$) with a sufficiently large electric field gradient (EFG), which is produced by a nonspherical charge distribution around the nuclear site, also affects the central NMR transition. Second order quadrupolar effects, influencing the shape of the NMR central line, cannot be (completely) eliminated by magic angle spinning. From the simulation of spectra recorded under MAS conditions, the quadrupole coupling constant

$$C_Q = eQV_{zz}/h$$

and the corresponding asymmetry parameter

$$\eta = (V_{xx} - V_{yy})/V_{zz}$$

can be estimated. Here, *e* is the positive elementary charge, *h* denotes Planck's constant, and V_{xx} , V_{yy} and V_{zz} are the elements of the traceless EFG tensor *V* with $|V_{zz}| \geq |V_{xx}| \geq |V_{yy}|$. V_{zz} = eq denotes its principal component. The shape of the NMR central line depends sensitively on the asymmetry of the electronic charge density close to the nucleus. The parameter η describes the deviation of the EFG from axial symmetry and it can take values between 0 and 1. Second order quadrupole interactions also affect the position of the NMR line in terms of a quadrupolar shift. A larger external magnetic field, however, lowers the effect. Here, we compute the EFG from the all-electron charge distribution without further approximation and C_Q is obtained using the nuclear quadrupole moment $Q(^{27}Al) = 1.616 \times 10^{-29}$ m^2 determined from the slope of the linear regression proposed by Body et al.[39] The data visualization were performed using the program VESTA.[40]

RESULTS

Crystal Chemistry of Al-bearing LLZO and Al^{3+} Partitioning Behavior. The most energetically favorable position of Al^{3+} in LLZO is at the tetrahedrally coordinated crystallographic special 24*d* position. Al^{3+} can be displaced toward a neighboring vacant general 96*h* site, which leads to a distortion of its oxygen coordination polyhedron. Calculated Al−O bond lengths for this coordination at 0 K are between 1.76 Å and 1.79 Å and the tetrahedral volume is 2.86 Å^3 (see Table 1).

Our calculations show that Al^{3+} at 96*h* is 4-fold coordinated, and distorted from tetrahedral coordination, with Al−O bond lengths varying from 1.76 to 1.92 Å, because of the displacement of Al^{3+} towards a vacant 24*d* site. Additionally, there are two O^{2-} ions further away that have on average approximately 1 Å longer bond distances. If they would be included in the local coordination sphere around Al^{3+}, a distorted octahedral coordination polyhedron with a volume of 16.33 Å^3 would result. The volume for the 4-fold coordinated polyhedron is 2.69 Å^3. Al^{3+} could also possibly be located at the special 48*g* site with three different pairs of Al−O bonds and calculated bond lengths of 1.93 Å, 2.00 Å and 2.12 Å, respectively, yielding a coordination volume of 10.67 Å^3. Any possible Al^{3+} at the 16*a* site would also be 6-fold coordinated with again three pairs of Al−O bonds with lengths of 1.90 Å, 2.03 Å, and 2.11 Å and a coordination volume of 10.69 Å^3. Al^{3+} at the 24*c* site would have four shorter Al−O bond lengths equal to 1.94 Å and four longer bonds of 2.84 Å length. This would give rise to a quasi-4-fold planar coordination for Al^{3+}. Assuming, on the other hand, 8-fold coordination around the 24*c* site, the resulting polyhedron would have a volume of 22.86 Å^3. The various hypothetical Al^{3+} coordination polyhedra at 0 K, along with their associated site preference energy, are shown in Figure 2.

Table 1. Various Calculated Interatomic Al−O Distances (d) [Å] and Coordination Polyhedra Volumes (V) [Å^3] in Cubic $Li_7La_3Zr_2O_{12}$

	24*d*	96*h*	48*g*	16*a*	24*c*
	Al−O	Al−O	Al−O	Al−O	Al−O
d	1.76	1.76	2.12	1.90	1.95
d	1.78	1.92	1.93	2.11	1.95
d	1.78	1.84	1.93	2.03	1.94
d	1.79	1.82	2.00	1.90	1.94
d		2.90	2.00	2.03	2.82
d		3.15	2.12	2.11	2.82
d					2.92
d					2.92
⟨d⟩	1.78	1.83[a]	2.02	2.01	1.94[a]
V	2.86	2.69[a]	10.67	10.69	22.86[b]

[a]Based on 4-fold coordination. [b]Based on 8-fold coordination.

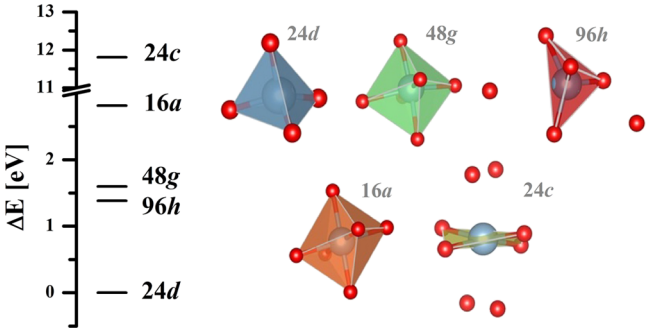

Figure 2. Various coordination polyhedral around Al^{3+} located at the 24*d*, 48*g*, 96*h*, 16*a*, and 24*c* sites. (Nonbonded red spheres indicate additional O^{2-} ions not considered as next nearest neighbors in the first coordination sphere. Their distances are given in Table 1.) Their associated site preference energies in cubic LLZO.

The calculated site preference energies, ΔE, for Al^{3+} in LLZO are as follows: 24*d* > 96*h* > 48*g* > 16*a* ≫ 24*c*. Al^{3+} at the 24*d* site has the global energy minimum and is 1.38 eV more stable than Al^{3+} at 96*h* and 1.60 eV more stable than Al^{3+} at 48*g*. The latter two sites are energetically similar with an energy difference of just 0.22 eV. The site preference energy for Al^{3+} at 16*a* and 24*c* is 0.41 and 1.74 eV higher, respectively, when referenced to the global energy minimum. The site preference energies for Al^{3+} at various structural positions between 48*g* and 24*d* are shown in Figure 3.

Calculated ^{27}Al NMR Parameters. Calculated ^{27}Al NMR parameters for Al^{3+} at the different structural sites in LLZO are shown in Table 2. The corresponding polyhedra (Figure 4) around Al^{3+}, slightly displaced from 24*d* and 96*h* (Figure 3),

dx.doi.org/10.1021/cm5000999 | Chem. Mater. 2014, 26, 2617−2623

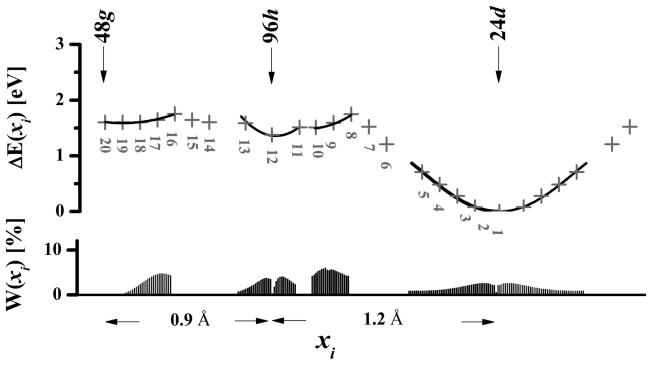

Figure 3. Site preference energies, ΔE, for Al^{3+} at various structural positions (gray crosses) at and near the 48*g*, 96*h* and 24*d* sites in LLZO garnet. The solid lines represent polynomial fits to the various ΔE values. The fits were used to calculate the Boltzmann distribution, $W(x_i)$ (see text), discussed below. The different distributions of Al^{3+} at the various crystallographic sites are normalized to 1 and indicate the room temperature probability of finding Al^{3+} at a distinct position.

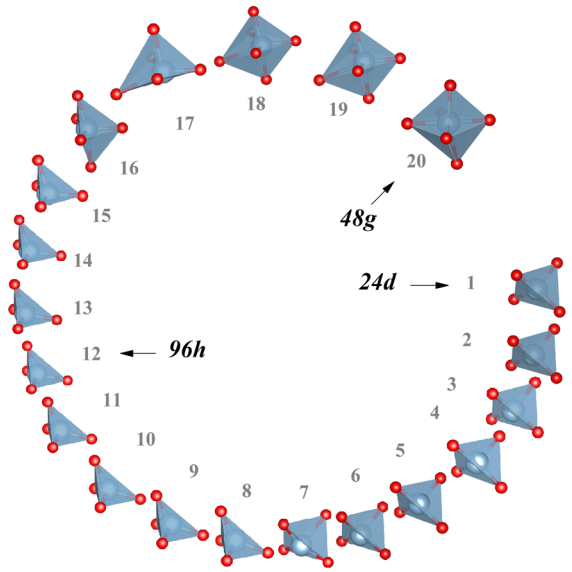

Figure 4. Oxygen coordination polyhedra around Al^{3+} for Al−O distances less than 2.6 Å at 17 local positions starting with 24*d* (1) and going to 96*h* (12) and beyond and ending at 48*g* (20) in cubic LLZO.

were used to analyze the experimental NMR spectra. The calculations show that Al^{3+} coordinations given by 1 to 5 (Figure 4) have $\Delta\delta$ values between −3.7 and 0.2 ppm, C_Q values between −1.38 and 5.01 MHz and η values between 0.20 and 0.70. Al^{3+} for coordinations given by 9 to 13 have $\Delta\delta$ values between 10.0 and 14.4 ppm, C_Q values between 2.4 and 3.3 MHz and η values between 0.24 and 0.70. On the other hand, Al^{3+} located at 48*g* has an extremely large calculated $\Delta\delta$ value of 133.5 ppm, 118.5 ppm at 24*c*, and 108.5 ppm at 16*a*. The latter three sites have δ values that are much larger than any experimentally observed NMR resonances.

DISCUSSION

In this DFT study, we investigated the crystal-chemical role of Al^{3+} in LLZO. Specifically, we address the question of the coordination and the site distribution behavior of Al^{3+}. The results of the calculations can be used, together with published experimental results, to achieve a better understanding of the nature of Al^{3+} incorporation in LLZO. We find that Al^{3+} at the 24*d* site is energetically the most stable state, followed by Al^{3+} at 96*h* and 48*g*, whereby the site preference energies for the latter two are similar. Al^{3+} at both the 16*a* and 24*c* sites is energetically unfavorable. Based on our DFT calculations, Al^{3+} should be exclusively located at 24*d* at 0 K, which would give rise to a single NMR resonance. Thus, the question arises why additional resonances are observed in the ^{27}Al MAS NMR spectra (Figure 5).[4−7]

Before discussing our results, we briefly outline the NMR results from the various studies with respect to the Al^{3+} site occupation in LLZO. In all recent studies the resonance at approximately 66 ± 2 ppm is assigned to Al^{3+} at the 24*d* site.[4−7]

Table 2. Calculated ^{27}Al NMR Parameters for Al^{3+} at Various Sites in Cubic $Li_7La_3Zr_2O_{12}$ Compared to Experimental Values from the Literature

	position[a]	δ[b] [ppm]	$\Delta\delta$[c] [ppm]	V_{ZZ}[d] [10^{21} V/m^2]	C_Q[e] [MHz]	η[f]	assignment
Geiger et al.[4]		68.0	13.0		5.0−5.2	0.0−0.1	24*d*
		81.0			3.3	0.7	96*h*
Buschmann et al.[5] and Düvel et al.[6]		64.0	14.0				24*d*
		78.0	18.0				
		82.0					
Hubaud et al.[7]		68.4			4.8	0.40	24*d*
		73.5	5.1		6.9	0.13	24*d*
Our calculations	1	68.0		−1.38	−0.8	0.10	24*d*
	2	68.2	0.2	2.14	1.3	0.94	
	3	64.3	−3.7	3.03	1.8	0.79	
	4	64.5	−3.5	3.97	2.3	0.71	
	5	64.8	−3.2	5.01	2.9	0.66	
	13	79.9	11.9	4.03	2.4	0.28	
	12	78.0	10.0	4.08	2.4	0.24	96*h*
	11	79.4	11.4	4.63	2.7	0.45	
	10	82.4	14.4	5.03	3.0	0.54	
	9	82.2	14.2	5.63	3.3	0.70	

[a]The position corresponds to Al^{3+} with the coordination polyhedra in Figure 4 and the site preference energies in Figure 3. [b]Calculated values are referenced to the global minimum given by δ = 68 ppm at position 1. [c]Literature: $\Delta\delta = \delta - \delta_{24d}$; Calculation: $\Delta\delta = \delta - 68$ ppm. [d]Principal component of the EFG. [e]Quadrupole coupling constant. [f]Asymmetry parameter.

dx.doi.org/10.1021/cm5000999 | Chem. Mater. 2014, 26, 2617−2623

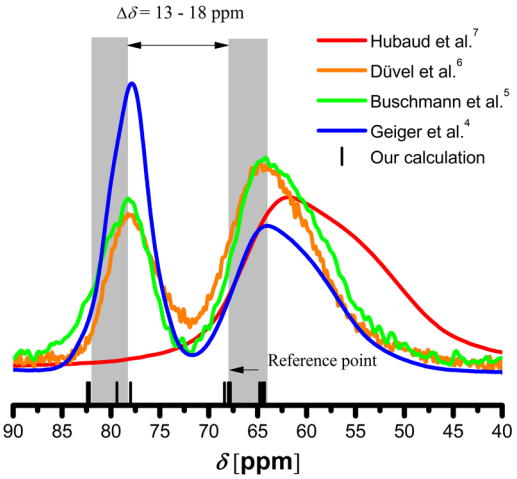

Figure 5. Experimental ^{27}Al NMR MAS spectra[4−7] compared to calculated δ values. The gray areas represent the variation in chemical shift values, $\Delta\delta$, (13 to 18 ppm) in literature. The reference point refers to $\Delta\delta$ = 0 given by the calculations.

Other NMR lines also indicate 4-fold coordinated Al^{3+} ions,[4−7] because their chemical shift values of 78 to 82 ppm are usually indicative of tetrahedral coordination. Geiger et al. assigned the resonance at 81 ppm to Al^{3+} residing at the 96*h* sites.[4] In particular, the spectra presented in ref 6 indicate that several NMR lines contribute to a signal occurring between 75 to 85 ppm. It should be noted that the latter has been reported for LLZO samples with a high amount of Al^{3+} and lower than stoichiometric La^{3+} and Zr^{4+} contents.[6] Such samples were prepared by mechanochemical activation combined with subsequent annealing at moderate temperatures.

Düvel et al. observed a stronger NMR signal at 64 ppm and a less intense line at 78 ppm for garnets with Al^{3+} contents up to 0.30 per formula unit (pfu). However, at concentrations above 0.60 Al^{3+} pfu the resonance at 78 ppm becomes the most intense. At even higher Al^{3+} contents a new NMR line at 81 ppm emerges, which notably appears in La- and Zr-deficient LLZO samples.

Geiger et al. made, in addition to ^{27}Al MAS NMR experiments, also ^{27}Al MQMAS NMR measurements.[4] The latter spectra show a resonance at δ = 81 ppm, a coupling constant, C_Q, of 3.3 MHz and an asymmetry parameter, η, of 0.7. These parameters indicate a strongly distorted local coordination geometry. The second resonance observed at δ = 68 ppm shows a stronger quadrupolar interaction with C_Q = 5.0 to 5.2 MHz and a lower η value between 0.0 and 0.1 that suggests axial symmetry at the site. It should be noted that the ^{27}Al MAS NMR spectrum was recorded at 156.26 MHz, thus providing a sufficiently high resolution to simulate its line shape. Such a simulation yields a resonance with δ = 81 ppm, C_Q = 3.3 MHz and η = 0.7, and for the second signal values of δ = 70 ppm, C_Q = 5.5 MHz and η = 0.5.

The calculated NMR parameters (Table 2) are in good agreement with an assignment of Al^{3+} to 96*h* for the resonance at 81 ppm. The calculated NMR parameters for the NMR line at 68 ppm that is assigned to Al^{3+} at 24*d*, however, disagree with those determined from the MQMAS NMR experiments. For the latter, it has been proposed that possibly more than one Al^{3+} site is reflected by this broad resonance. This possibility was underlined by Hubaud et al.[7] They made ^{27}Al MQMAS NMR spectroscopic measurements to investigate this resonance at 68 ppm for an Al-doped LLZO garnet synthesized at 850 °C. Their line shape analysis yielded two NMR lines with the first having δ = 68.4 ppm and C_Q = 4.8 MHz and the second δ = 73.5 ppm and C_Q = 6.9 MHz. Both resonances were assigned to tetrahedrally coordinated Al^{3+} at 24*d* in two different garnet phases. The two tetrahedral sites have slightly different distortions and thus different δ and C_Q values. Hubaud et al. report that this interpretation is consistent with their high-resolution XRPD results, and they proposed that slow Al^{3+} diffusion within the lattice is responsible for the disordering over the two sites.

Our DFT calculations permit a somewhat different interpretation of the experimental results. For the first step, we calculated the NMR parameters for Al^{3+} at all crystallographic sites, via 24*d*, 48*g*, 96*h*, 16*a*, and 24*c*. According to our results, the resonance at 80 ± 2 ppm should be assigned to Al^{3+} residing at the 96*h* sites and the resonance at 66 ± 2 ppm to Al^{3+} occupying 24*d*. These results agree with interpretations of experimental NMR spectra.[4−6] There is good agreement between the calculated C_Q value for Al^{3+} at 96*h*, but disagreement between C_Q values for Al at 24*d*. Hubaud et al. proposed a large C_Q value for Al^{3+} at 24*d*, but it cannot be easily explained why the symmetric 24*d* site should yield a C_Q value approximately two times larger than Al^{3+} at the more distorted 96*h* site.[7]

To understand this issue better, we calculated the NMR parameters for Al^{3+} at all positions at and around 24*d* and 96*h* that are occupied by a certain probability. Shifting Al^{3+} away from 24*d* and 96*h* leads to a distribution of slightly different local oxygen coordination environments. Thereby, broad ^{27}Al MAS NMR resonances could result, which would reflect a distribution of slightly different δ and C_Q values. We note that our calculations for η for Al^{3+} at 24*d* do not agree with experiment, but η was obtained from the experimental spectra by using only one[4] or two[7] Al^{3+} resonances to simulate this broad feature at 66 ± 2 ppm.

The NMR signal located at 78 to 82 ppm is also asymmetric in shape. This is possibly due to the slightly different geometries of local Al^{3+} coordinations, as given by their calculated probabilities, toward the 48*g* minimum versus those in the direction of 24*d*. This situation could produce two overlapping resonances having similar values of δ and C_Q (see also the agreement with experimental results and the discussion in ref 6).

Although experiment and calculations are in broad agreement in terms of the crystal chemical role of Al^{3+} in LLZO, it is not clear based on the DFT calculations alone, why Al^{3+} is not located exclusively at 24*d*[6] as suggested by the site energies. Al^{3+} at 96*h* and 48*g* must also be considered, which, however, would lead to an additional NMR line which is usually not observed experimentally. (For the sake of completeness, let us note that an additional NMR line has been observed at 93 ppm for Al-doped $Li_{6.5}La_{2.5}Ba_{0.5}ZrTaO_{12}$ [42] and for some of the Al-doped LLZO samples prepared via mechanosynthesis [6]; the prominent NMR line at 65 ppm, however, is absent in these cases.) Here, it must be stated that the exact thermodynamic state of LLZO, as obtained in the various sintering experiments, is not known. It is possible that metastable structural states are obtained that can depend on a number of experimental factors (dopant concentration, sintering temperature and time, heating rate, grain sizes, starting materials, etc.). Thus, Al^{3+} could potentially be incorporated metastably at 96*h* and 48*g* as well in cubic LLZO, because both sites have similar site energies.

dx.doi.org/10.1021/cm5000999 | *Chem. Mater.* 2014, 26, 2617−2623

The different site energies for Al^{3+} at 24*d* and 96*h* could provide an explanation for differences in published NMR spectra of LLZO. The relationship between Al^{3+} concentration and variations in the intensities of the different resonances (and thus Al^{3+} site occupancies), as observed by Düvel et al., can be interpreted crystal chemically. When an Al^{3+} ion is located at 24*d*, because of its large effective charge radius, it could create a larger inaccessible region around 24*d* compared to the situation for Al^{3+} at 96*h*. This region cannot be occupied by other ions. This leads to a reduction of entropy and a loss of energy possibly making the 96*h* site energetically more accessible for Al^{3+} with increased Al^{3+} contents in contrast to the 24*d* site. Similar considerations were made by Bernstein et al.[36] They showed by using molecular dynamics simulations that the introduction of vacancies in LLZO does indeed reduce the free energy. This indirectly supports our suggestion.

Lastly, we consider the coordination geometry around the 96*h* site in LLZO, which has been described differently.[4,11,23] It is, of course, a matter of definition as to what constitutes a bond in a first coordination sphere. According to Li et al. in their description of Al at 96*h*, the average Al−O bond distance is $d^{[4]}$ = 2.08 Å, with a difference of 0.38 Å between the length of the shortest and the longest bonds. There are two further O^{2-} ions that give Al−O = 2.69 Å and 2.80 Å, thus being 0.46 Å and 0.57 Å longer compared to the longest bond in strict 4-fold coordination. Based on our calculations, Al^{3+} at 96*h* has a locally 4-fold distorted coordination (Figure 4). It is worth mentioning that long-range structural properties, as determined by the diffraction experiment, such as neutron powder diffraction, can differ from those measured via spectroscopy, for example, NMR, which probes structure at shorter length scales.

CONCLUSION

Based on our DFT results, we propose that Al^{3+} could have a number of slightly different local 4-fold coordinations around the crystallographic 24*d* and 96*h* sites in cubic LLZO garnet. The calculations are in general agreement with published experimental ^{27}Al NMR spectra. It should be noted further that Li et al.,[11] in a neutron diffraction study of cubic LLZO garnet, proposed that Al^{3+} is located at the 48*g* site in octahedral coordination. In terms of calculated site energies, this site could be partially occupied. However, the calculated Al NMR chemical shift value for such coordination has not been observed in experimental NMR spectra.

AUTHOR INFORMATION

Corresponding Author

*E-mail: daniel.rettenwander@sbg.ac.at.

Notes

The authors declare no competing financial interest.

ACKNOWLEDGMENTS

We thank M. Grodzicki (University Salzburg) for discussions and the CHPC Salzburg, especially Peter Zinterhof junior (University of Salzburg), and the HPC-EUROPA2 project (project number: 1212) for support within the European Commission Capacities Area, Research Infrastructures Initiative. This research was made possible by the Austrian Science Fund (FWF) through project number P25702. M.W. thanks the Austrian Federal Ministry of Economy, Family and Youth, and the Austrian National Foundation for Research, Technology, and Development for financial support. Thanks also go to John T. Vaughey and Baris Key (Argonne National Laboratory) for providing their NMR spectra (ref 7).

REFERENCES

(1) Murugan, R.; Thangadurai, V.; Weppner, W. *Angew. Chem.* **2007**, *119*, 7925.
(2) Awaka, J.; Kijima, N.; Hayakawa, H.; Akimoto, J. *J. Solid State Chem.* **2009**, *182*, 2046.
(3) Awaka, J.; Takashima, A.; Hayakawa, H.; Kijima, N.; Idemoto, Y.; Akimoto, J. *Key Eng. Mater.* **2011**, *485*, 99.
(4) Geiger, C. A.; Alekseev, E.; Lazic, B.; Fisch, M.; Armbruster, T.; Langner, R.; Fechtelkord, M.; Kim, N.; Pettke, T.; Weppner, W. *Inorg. Chem.* **2011**, *50*, 1089.
(5) Buschmann, H.; Dölle, J.; Berendts, S.; Kuhn, A.; Bottke, P.; Wilkening, M.; Heitjans, P.; Senyshyn, A.; Ehrenberg, H.; Lotnyk, A.; Duppel, V.; Kienle, L.; Janek, J. *Phys. Chem. Chem. Phys.* **2011**, *13*, 19378.
(6) Düvel, A.; Kuhn, A.; Robben, L.; Wilkening, M.; Heitjans, P. *J. Phys. Chem. C* **2012**, *116*, 15192.
(7) Hubaud, A. A.; Schroeder, D. J.; Key, B.; Ingram, B. J.; Dogan, F.; Vaughey, J. T. *J. Mater. Chem. A* **2013**, *1*, 8813.
(8) Rangasamy, E.; Wolfenstine, J.; Sakamoto, J. *Solid State Ionics* **2012**, *206*, 28.
(9) Kanamura, K.; Kaeriyama, A.; Honda, A.; Yoshida, T.; Sato, Y. US patent 20110053000, 2011.
(10) Kotobuki, M.; Kanamura, K.; Sato, Y.; Yoshida, T. *J. Power Sources* **2011**, *196*, 7750.
(11) Li, Y.; Han, J.-T.; Wang, C.-A.; Vogel, S. C.; Xie, H.; Xu, M.; Goodenough, J. B. *J. Power Sources* **2012**, *209*, 278.
(12) Kuhn, A.; Choi, J.-Y.; Robben, L.; Tietz, F.; Wilkening, M.; Heitjans, P. *Z. Phys. Chem.* **2012**, *226*, 525.
(13) Jin, Y.; McGinn, P. J. *Electrochim. Acta* **2013**, *89*, 407.
(14) Jin, Y.; McGinn, P. J. *J. Power Sources* **2011**, *196*, 8683.
(15) Wolfenstine, J.; Sakamoto, J.; Allen, J. L. *J. Mater. Sci.* **2012**, *47*, 4428.
(16) Tietz, F.; Wegener, T.; Gerhards, M. T.; Giarola, M.; Mariotto, G. *Solid State Ionics* **2013**, *230*, 77.
(17) Matsui, M.; Takahashi, K.; Sakamoto, K.; Hirano, A.; Takeda, Y.; Yamamoto, O.; Imanishi, N. *Dalton Trans.* **2014**, *43*, 1019.
(18) Cheng, L.; Park, J. S.; Hou, H.; Zorba, V.; Chen, G.; Richardson, T.; Cabana, J.; Russo, R.; Doeff, M. *J. Mater. Chem. A* **2014**, *2*, 172.
(19) Sudo, R.; Nakata, K.; Ishiguro, K.; Matsui, M.; Hirano, A.; Takeda, Y.; Yamamoto, O.; Imanishi, N. *Solid State Ionics* **2013**, article in press.
(20) Cussen, E. *J. Mater. Chem.* **2010**, *20*, 5167.
(21) Menzer, G. *Z. Kristallogr.* **1928**, *69*, 300.
(22) Hellner, E.; Gerlich, R.; Koch, E.; Fischer, W. *Physics Data*; Fachinformationszentrum Energie, Physik, Mathematik: Karlsruhe, Germany, 1979; *16*−*1*: 1−16.
(23) Percival, J.; Kendrick, E.; Smith, R. I.; Slater, P. R. *Dalton Trans.* **2009**, *26*, 5177.
(24) Xie, H.; Alonso, J. A.; Li, Y.; Fern, M. T.; Goodenough, J. B *Chem. Mater.* **2011**, *23*, 3587.
(25) Xu, M.; Park, M. S.; Lee, J. M.; Kim, T. Y.; Park, Y. S.; Ma, E. *Phys. Rev. B* **2012**, *85*, 052301.
(26) Bernstein, N.; Johannes, M. D.; Hoang, K. *Phys. Rev. Lett.* **2012**, *109*, 205702.
(27) Nakayama, M.; Kotobuki, M.; Munakata, H.; Nogami, M.; Masayuki, K.; Kanamura, K. *Phys. Chem. Chem. Phys.* **2012**, *14*, 10008.
(28) Jalem, R.; Yamamoto, Y.; Shibba, H.; Nakayama, M.; Munakata, H.; Kasuga, T.; Kanamura, K. *Chem. Mater.* **2013**, *25*, 425.
(29) Miara, J. L.; Ong, S. P.; Mo, Y.; Richards, W. D.; Park, Y.; Lee, J.-M.; Lee, H. S.; Ceder, G. *Chem. Mater.* **2013**, *25*, 3048.
(30) Madsen, G. K. H.; Blaha, P.; Schwarz, K.; Sjöstedt, E.; Nordström, L. *Phys. Rev. B* **2001**, *64*, 195134.
(31) Blaha, P.; Schwarz, K.; Madsen, G. K. H.; Kvasnicka, D.; Luitz, J. *WIEN2K*, Version 13.1; An Augmented Plane Wave + Local Orbital

Program for Calculating Crystal Properties; Technical University: Vienna, Austria, 2001.
(32) Perdew, J . P.; Burke, K.; Ernzerhof, M. *Phys. Rev. Lett.* **1996**, *77*, 3865.
(33) Marks, L. D. *J. Chem. Theor. Comput.* **2013**, *9*, 2786.
(34) Blaha, P.; Hofstätter, H.; Koch, R.; Laskowski, R.; Schwarz, K. *J. Comput. Phys.* **2009**, *229*, 453.
(35) Maricq, M. M.; Waugh, J. S. *J. Chem. Phys.* **1979**, *70*, 33003316.
(36) Laskowski, R.; Blaha, P. *Phys. Rev. B* **2012**, *85*, 035132.
(37) Laskowski, R.; Blaha, P.; Tran, F. *Phys. Rev. B* **2013**, *87*, 195130.
(38) Laskowski, R.; Blaha, P. *Phys. Rev. B* **2014**, *89*, 014402.
(39) Body, M.; Legein, C.; Buzare, J.-Y.; Silly, G.; Blaha, P.; Martineau, C.; Calvayrac, F. *J. Phys. Chem. A* **2007**, *111*, 1187.
(40) Momma, K.; Izumi, F. *J. Appl. Crystallogr.* **2011**, *44*, 1272.
(41) Narayanan, S.; Epp, V.; Wilkening, M.; Thangadurai, V. *RSC Adv.* **2012**, *2*, 2553.